Published in final edited form as:

J Chem Inf Model. 2019 June 24; 59(6): 2952–2963. doi:10.1021/acs.jcim.9b00217.

Conformation and Permeability: Cyclic Hexapeptide Diastereomers

Satoshi Ono[*,†], **Matthew R. Naylor**[‡], **Chad E. Townsend**[‡], **Chieko Okumura**[†], **Okimasa Okada**[†], **R. Scott Lokey**[*,‡]

[†]Modality Laboratories, Innovative Research Division, Mitsubishi Tanabe Pharma Corporation, 1000, Kamoshida-cho, Aoba-ku, Yokohama, Kanagawa 227-0033, Japan

[‡]Department of Chemistry and Biochemistry, University of California Santa Cruz, 1156 High Street, Santa Cruz, California 95064, United States

Abstract

Conformational ensembles of eight cyclic hexapeptide diastereomers in explicit cyclohexane, chloroform and water were analyzed by multicanonical molecular dynamics (McMD) simulations. Free energy landscapes (FELs) for each compound and solvent were obtained from the molecular shapes and principal component analysis at T = 300 K; detailed analysis of the conformational ensembles and flexibility of the FELs revealed that permeable compounds have different structural profiles even for a single stereoisomeric change. The average solvent accessible surface area (SASA) in cyclohexane showed excellent correlation with the cell permeability, whereas this correlation was weaker in chloroform. The average SASA in water correlated with the aqueous solubility. The average polar surface area did not correlate with cell permeability in these solvents. A possible strategy for designing permeable cyclic peptides from FELs obtained from McMD simulations is proposed.

Graphical Abstract

[*]**Corresponding Authors**: ono.satoshi@mg.mt-pharma.co.jp. slokey@ucsc.edu.

The authors declare no competing financial interest.

ASSOCIATED CONTENT

Supporting Information

Figures S1 to S3: Free energy landscapes of (ϕ,ψ) for each solvent; Figures S4 to S11: Backbone H-bond patterns of each compound and solvent; Figure S12: Free energy landscapes for PC-1 and PC-3; Figure S13: $LogD_{cyc/w}$ vs. average SASA and PSA for each solvent; Figure S14: Representative structures of β-turn pattern F and G; Figure S15: Overlaps between the FELs from the PC plane; Figure S16: Free energy landscapes of (ϕ,ψ) for known cyclic peptides; Tables S1 to S3: Zones for virtual states and real potential energy for each solvent; Table S4: Backbone (phi, psi) values for representative structures shown in Figure 4. (PDF)

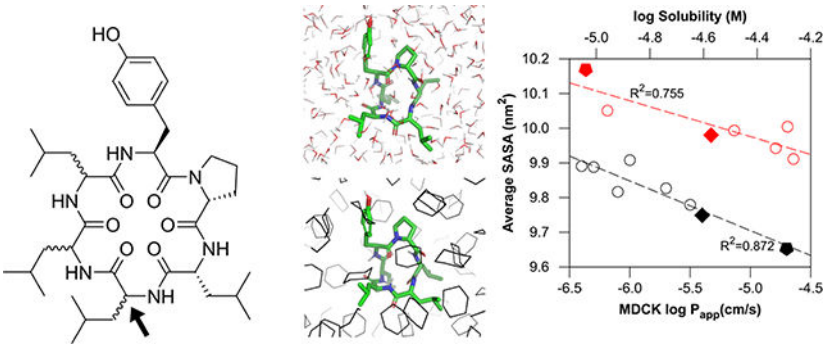

1. INTRODUCTION

Efficient conformational sampling of macrocycles is an emerging interest for assigning physical properties, especially for modalities in “beyond the rule-of-five (bRo5)” chemical space, such as cyclic peptides.[1–14] Conventional sampling methods have been performed in implicit solvent using molecular mechanics to predict, for example, membrane permeability.[6,7] Because cyclic peptides have many metastable states in solvents, selecting single conformations for molecular property assignment may be insufficient, requiring more powerful sampling methods. Recently, replica exchange molecular dynamics (REMD),[15] metadynamics (MetaD),[16] and accelerated MD (aMD)[17] simulations in explicit solvent were adopted to investigate relationships between the detailed structure of cyclic peptides and their physical properties, such as cell permeability, aqueous solubility,[9,10] and structural and thermodynamic information.[11–14] Although these methods are generally used, exchange rate optimization is required for REMD simulations, and many collective variables are required for MetaD simulations. Other approaches denoted CANDLE,[18] which combines molecular dynamics and quantum mechanics, BRIKARD,[19] an inverse kinematics method, and EGSCyP,[20] a robotics based method, were used to determine cyclic peptide conformations.

Multicanonical molecular dynamics (McMD)[21] simulation is a powerful enhanced sampling method in which the potential energy is equally sampled between low and high temperature regions. By reweighting the entire set of sampled structures, the canonical ensemble can be obtained at any temperature provided that it is between the low and high temperature states (Figure 1). McMD simulations and their derivatives have been successfully applied to small peptides,[22–24] intrinsically disordered protein (IDP),[25,26] antibody CDR-H3 loop,[27] and protein-ligand docking simulations[28] in explicit water.

It is noteworthy that solvent selection is important for conformational effects in both computation and experiments. Conventionally, conformational sampling in chloroform has been used to mimic the membrane environment in a low dielectric solvent for both implicit ($\varepsilon = 4$)[7] and explicit models.[8,29] Recently, experimental hydrocarbon–water distribution coefficients, $\log D_{hc/w}$, showed excellent correlation with cell permeability,[30] suggesting that hydrocarbons, such as cyclohexane, can be alternative solvents for mimicking membrane environments. The steep demands of conformational chameleonicity[31–33] for favorable pharmacokinetic properties in bRo5 chemical space will also require calculation of the conformations in water to determine conformationally defined aqueous solubility.

To test the hydrophobic environment, conformations of eight cyclic hexapeptide diastereomers (Figure 2 and Table 1)[34] were investigated in explicit cyclohexane, chloroform and water. Although the molecular properties of these cyclic peptides, such as molecular weight (MW) = 712.93, topological polar surface area (TPSA)[35] = 186.04, and predicted hydrophobic partition coefficient AlogP[36] = 3.82, were identical, the cell permeability in a low-efflux MDCK cell line[37] varied by over two orders of magnitude. Remarkably, these cyclic peptides have no N-methylated amino acid groups, which is considered a key feature in enhanced cell membrane permeability, as these either mask the polar amide group or stabilize the *cis* isomer.[38–40] We have applied McMD simulations to cyclic peptides as an effective conformational sampling method and thermodynamically stable conformations were obtained through analysis of the free energy landscape (FEL). We expected that the thermodynamically stable conformer of these cyclic hexapeptide diastereomers would have different 3D structures in the solvents to explain the differences in cell permeability. We mainly focused on the thermodynamic behavior of these compounds in bulk solvents from simulations and did not treat the atoms in the membrane explicitly (*e.g.*, conformational changes upon binding to polar head groups of the membrane were not considered).

Selecting the force field for cyclic peptides is another issue,[41,42] because current force fields were mainly tailored to linear peptides and proteins in water. A previous study showed that force field reparameterization may be required for cyclic peptides.[41] Because our preliminary study revealed that the AMBER force field ff03[43] effectively reproduces the NMR or X-ray structure of known cyclic peptides, we adopted ff03 in the present research.

2. METHODS

2.1 Simulation details.

The initial conformer was built using the MOE[44] protein builder, and LowModeMD[45] implemented in MOE was used to search for the most stable conformer in vacuo. PACKMOL[46] was used to solvate the system, where the numbers of water, chloroform, and cyclohexane molecules were 2000, 400, and 300, respectively. The TIP3P water model[47] and chloroform from AmberTools17[48] were used. For cyclohexane, the atom types cD and hL from the Lipid14 force field[49] and RESP ESP charges from R.E.D. version III.52[50] were used. The AMBER ff03 force field[43] was used for amino acids. The topology file was created using the LEaP program and converted to GROMACS format using the ParmEd program in AmberTools17. The initially solvated system was minimized by steepest descent, following 50,000 steps of NVT calculation. The system was then equilibrated by NPT calculation at atmospheric pressure by applying the Berendsen barostat[51] for 500,000 steps. A positional restraint was used for C_α atoms during equilibration. The resultant system was used as an initial structure for the following simulations.

Virtual-system-coupled Trivial Trajectory Parallelization of Multicanonical Molecular Dynamics (TTP-V-McMD)[52,53] simulations were adopted to effectively sample conformations of cyclic peptides. TTP-V-McMD is a derivative and combination of Trivial Trajectory Parallelization McMD (TTP-McMD)[52] and Virtual-system-coupled McMD (V-McMD),[53] where TTP-McMD consists of several multiple independent McMD runs with

same McMD parameters from different initial conformations. V-McMD consists of several virtual states with independent McMD parameters that cover different potential energies, where neighboring virtual states overlap. In this report, the term "McMD simulations" denotes "TTP-V-McMD simulations," because TTP-V-McMD is a derivative of McMD. A total of 336 pre-TTP-V-McMD runs were initiated with random velocities for each atom at T = 300 K, then heated to T = 1525 K with 5,000 steps, followed by 495,000 steps at T = 1525 K to randomize the initial structures. To determine the potential energy zones for McMD, following pre-TTP-V-McMD runs were conducted at 14 temperatures; 1525 K, 1203 K, 1002 K, 802 K, 707 K, 633 K, 573 K, 501 K, 445 K, 400 K, 354 K, 325 K, 300 K, and 280 K. Then the virtual state zones and real potential energy zones were set as listed in Table S1 to S3. The transition probability to neighboring virtual states was set to 1.0. Because McMD parameters are not known *a priori*, we need some iterations to determine those parameters. For each virtual state, the McMD parameter was fitted to an eighth order polynomial curve according to the equation 24 in Ref. 53. Flat potential energy distributions between T = 1525 K and 280 K were obtained by iterating TTP-V-McMD simulations for five times in chloroform and water, or six times in cyclohexane with eight virtual states (See detail in Figure 3). The cut-off for coulombic and van der Waals interactions was 1.0 nm, and PME was used to calculate the long-range electrostatics. The NVT ensemble was used for all TTP-V-McMD simulations using the velocity rescaling method (Bussi thermostat).[54] The LINCS algorithm[55] was used to constrain the bonds with a hydrogen atom, allowing time steps of 2.0 fs. For each compound and solvent, 1.0×10^7 steps × 336 runs (Total 6.72 μs) were performed as a final production run. The structure and potential energy were stored every 2 ps. The virtual state was exchanged in every 5,000 steps. Solvent atoms were removed before analysis. For cluster and property analysis, a resampling method was used to extract the canonical ensemble at T = 300 K, where structures were drawn from the simulated ensemble with relative probabilities according to their Boltzmann weights. Typically, approximately 18,000 conformers were obtained, and then 5,000 conformers were randomly selected to use for further cluster and property analysis. All 3.36 million conformers were taken into account to determine the FEL by a potential of mean force (PMF) calculation; $W = -k_B T \ln \rho$, where k_B is the Boltzmann constant and ρ is the density of state.[56] An in-house implemented TTP-V-McMD using GROMACS[57] version 5.1.4 was used for the simulations. The density of the bulk solvents was confirmed by NPT ensemble at T = 300 K. The calculated densities for water, chloroform and cyclohexane were 0.984, 1.470, and 0.771 g/cm^3, respectively, which are close to the experimental values.

2.2 Clustering analysis.

TTClust[58] was used to cluster each ensemble. Backbone root mean square deviation (RMSD) was used to obtain a distance matrix. The Ward method[59] was used for hierarchical clustering. A total of 5,000 structures obtained for a T = 300 K ensemble of each compound and solvent, were divided into 1,000 structures × 5 groups to calculate the standard deviations of each cluster. Some trials were performed to determine the optimal number of clusters (*i.e.*, N = 3 or 5). After inspecting the cluster analysis dendrograms and FELs, we set the cluster number to five for all clustering analyses to automate the TTClust script. The clusters which had same conformation were then combined to one, if exist. The pattern of

backbone-backbone H-bonds was calculated by VMD[60] with a donor-acceptor atomic distance below 0.35 nm and an angle cut-off (D-H … A) below 30 degrees.

2.3 Property calculation.

Principal moments of inertia (PMI) around inertial axes, $\mathbf{I_1}$, $\mathbf{I_2}$ and $\mathbf{I_3}$ were obtained in GROMACS using the command gmx principal. The molecular shape[61] was represented by the normalized PMI ratios ($\mathbf{I_1/I_3}$ and $\mathbf{I_2/I_3}$) for each frame. The surface area was obtained in GROMACS using gmx sasa. The solvent accessible surface area (SASA) was defined by all the atoms of the cyclic peptide. The polar surface area (PSA) was defined by nitrogen, oxygen, and hydrogen atoms attached to either a nitrogen or an oxygen atom of amino acids. The radius of the solvent probe was set to 0.14 nm. The average SASA and PSA were calculated for each compound and solvent for 5,000 structures by simply arithmetically averaging, because these structures were already Boltzmann weighted.

A new flexibility index denoted $Flex_{FEL}$ is introduced by,

$$Flex_{FEL} = \sum_{x,y} \Delta\, d(x,y) \cdot A \cdot \exp\left\{-\frac{W(x,y)}{k_B T}\right\} \quad (1)$$

where Δd(x, y) is the distance between the global minimum of the FEL and the coordinate (x, y), A is the unit area of the FEL, and W(x, y) is the PMF value at position (x, y). $Flex_{FEL}$ is considered as the area weighted by the extent of the PMF in the FEL. Based on this definition, a rigid conformation shows a small $Flex_{FEL}$ value, whereas this is larger for a flexible conformation.

The overlap between the FELs is defined by,

$$Overlap_{s1 \to s2}(z) = \sum_{x,y} A \cdot \exp\left\{-\frac{W_{s2}(x,y) \cap (W_{s1}(x,y) \le z)}{k_B T}\right\} \quad (2)$$

where *s1*, *s2*, and *z* are solvent 1, solvent 2, and the PMF threshold, respectively. The overlap value represents the weighted area of the FEL in solvent 2, where the PMF in solvent 1 is less than threshold *z*.

2.4 Experimental section.

The PAMPA permeability was obtained as described in Ref. 30. Briefly, a membrane was prepared on a 96-well filter support (donor) with a 1% (w/v) solution of lecithin (soybean) in n-dodecane. Analytes were dissolved to 1 μM in pH = 7.4 phosphate-buffered saline containing 5% dimethyl sulfoxide applied to the donor well and placed on a Teflon acceptor plate prepared with the same solution without analyte. After incubation for ~16 h, the donor and acceptor plates were separated and quantified via LCMS, via extracted ions.

3. RESULTS and DISCUSSION

3.1 Sampling efficiency.

McMD simulations are usually performed with a flat potential energy region that corresponds to a temperature between 280 and 700 K for linear peptides and small proteins.[22–28] In the present study, we set the temperature between 280 and 1525 K to improve the sampling efficiency for conformationally restricted cyclic peptides in which a higher rotation free energy may be required. It was also expected that setting the highest potential energy region corresponding to T = 1525 K would be required to ensure *cis/trans* isomerization of proline.[62] The resulting flat potential energy distributions and exchanges between virtual states revealed that McMD simulations sampled potential energy space adequately (Figure 3). The FELs of the backbone (ϕ,ψ) maps for each amino acid (Supporting Information Figures S1 to S3) also revealed that the simulations sampled conformational space adequately even though the relaxation time in cyclohexane is longer than in water and chloroform.

A previous study showed that *trans* to *cis* amide isomerization was observed in high temperature MD.[63] Since we set the flat potential energy region corresponding to the temperature between 1525 and 280 K, *cis/trans* isomerization was frequently observed, especially between L-Tyr6 and D-Pro1. However, reweighted ensembles at T = 300 K had minimal *cis* isomers for non-proline residues (*e.g.*, PMF of the *cis* isomer was 3.6 kcal/mol or more where the *trans* isomer was 0.0 kcal/mol for compound **7** in chloroform), whereas for proline, the *cis* isomer was much favored (*e.g.*, PMF of *cis* isomer was 2.0 kcal/mol for compound **7** in cyclohexane). We also confirmed the absence of continuous chiral inversion for each amino acid.

3.2 Intramolecular hydrogen bond (IMHB) patterns and 3D structures.

From analyzing ensembles at T = 300 K, we found five major backbone transannular H-bonding patterns, mainly in cyclohexane and chloroform (Table 2, Figure 4 and Supporting Information Figures S4 to S11). These five representative structures were extracted from the cluster analysis, namely a cage-like pattern (nIMHB (the number of IMHB) = 3 and 4 corresponding to **A** and **B**, respectively. See Table 2 and Figure 4), β-turn pattern (nIMHB = 2, corresponding to **C**), and collapsed β-turn pattern (nIMHB = 5, corresponding to **D** and **E**). The rest of the population remaining unclassified was mainly attributed to nIMHB = 0 or 1. Cage-like patterns exhibited one or two exposed NH amides and β-turn patterns had three exposed NH amides, whereas the collapsed β-turn had no exposed NH amides. An L-Tyr6-D-Pro1 β-turn corresponding to the matrix [2, 5] (Donor-Acceptor residue occurrence map in Figure 4) commonly appeared for five representative structures. H-bonding [4, 6] never appeared for D-Leu4 stereoisomers due to steric occlusion of Leu (over its NH) for all the obtained structures. These compounds (**1** to **4**) could only form collapsed β-turn pattern **D** in cyclohexane and chloroform. However, L-Leu4 stereoisomers (**5** to **8**) could form collapsed β-turn pattern **E**. Matrix [5, 3] also never appeared for D-Leu4 and D-Leu5 (compounds **2** and **4**), suggesting that these compounds could only form cage-like pattern **A**. L-Leu5 stereoisomers (compounds **1**, **3**, **5**, and **6**) could form cage-like pattern **B** in cyclohexane and

chloroform. The side chain hydroxyl group of Tyr6 rarely formed a hydrogen bond to the backbone, its occurrence being less than 0.22%.

However, the IMHB patterns in water were sparse, and hydrogen bond occupancy was lower than in cyclohexane and chloroform (Table 2 and Figures S4 to S11). This was because amide NH could form a hydrogen bond with water molecules, decreasing the occurrence of transannular H-bonding. Only compound **6** yielded no patterns in water, unlike its single stereoisomers **3**, **5**, and **8**. Other β-turn-like patterns that were not attributed to **A** to **E** were observed in minor clusters, where hydrogen bonds were formed between Tyr6 and Leu3 (Pattern **F**, corresponding to hydrogen bond matrices [3,6] and [6,3]. See cluster 5 in water of **6** in Figures S9 and S14) and between Leu4 and D-Pro1 (Pattern **G**, matrix [4,1], cluster 1 in water of **5** in Figures S8 and S14). However, these β-turns were rarely observed in cyclohexane and chloroform, because their Pro-Tyr backbone β-turn and side-chain–side-chain interactions are effectively stabilized in these solvents.

In a previous NMR study on the exposure of amide NH obtained from $\Delta\delta/\Delta T$[64] in $CDCl_3$ (Table S10 of Supporting Information in Ref. 34), one of the amide hydrogens of compound **3** is clearly exposed to the solvent, which supports the cage-like pattern (**B**), whereas no amide hydrogen is exposed for compounds **7** and **8,** supporting the collapsed β-turn pattern (**E**). Therefore, it was considered that McMD simulations with the AMBER ff03 force field appropriately sampled the diastereomeric structures.

3.3 Free energy landscapes of molecular shape and principal component analysis.

The molecular shape[61] was defined by the normalized principal moment of inertia and represented by 2D triangular graphs where the left top corner was rod-like, the right top corner sphere-like, and the bottom disk-like. Although these graphs were used to compare the shapes of fragments or combinatorial libraries of molecules, we applied this method to MD trajectories to represent the FEL of molecular shape (Figure 5a–c). It is noteworthy that the FEL exhibits a molecular shape distribution for cyclic peptides, rather than a single point. The FELs clearly showed that all the compounds adopt relatively rigid sphere-like conformations in cyclohexane but more flexible shapes in water. For example, compound **7** is sphere-like in cyclohexane; however, various shapes are formed in water. The FELs in chloroform were mostly the same as those in cyclohexane, except for compounds **5** and **7**. We will discuss the effect of solvents in detail later. Characteristic shapes of FELs in water were disk-like to disk-rod-like, whereas these shapes never appeared in cyclohexane. Disk-like compounds **4** and **8** were flat overall. These shapes were similar to that of a cyclic peptide nanotube,[65–67] with four out of the five NH amides being almost perpendicular to the backbone circle, whereas side-chains were in-plane. (See Figure 4c).

The FEL along with the principal component axes was drawn for each compound and solvent (Figures 6 and S12). The distance matrix was calculated from the distances between C_α atoms of each residue. Portions of variances are 36.7%, 28.9%, and 23.1% for the first, second, and third axes, respectively. From inspecting the coordinates and represented conformations by cluster analysis, the FELs showed the relations to the backbone H-bonding patterns describe below. A stable conformation around (PC-1, PC-2) = (0.1, −0.05) is a

cage-like pattern (**A** and **B** in Figure 4), (PC-1, PC-2) = (−0.05, −0.15) a β-turn pattern (**C**), (PC-1, PC-2) = (0.05, 0.1) a collapsed β-turn pattern (**D**), and (PC-1, PC-2) = (0.12, 0.1) another collapsed β-turn pattern (**E**). Relatively small free energy differences (<1 kcal/mol) were observed between cage-like and β-turn patterns (*e.g.,* compound **5**); however, large free energy differences (*ca.* 3 kcal/mol) were observed between β-turn and collapsed β-turn patterns (*e.g.,* compound **7**). Both conformational changes occurred by peptide-plane flips[68] of D-Leu2 and D-Leu3 for compounds **5** and **7**. Other β-turn patterns that are not classified above were **F** (PC-1, PC-2) = (−0.25, 0.25) and **G** (−0.18, 0.05). A disk-like conformation was located around (PC-1, PC-2) = (−0.3, 0.1) (**H** in Figure 6d).

Various conformations in water were found in the FELs of both molecular shape and principal component analysis compared to those in cyclohexane and chloroform. The most structured conformation found in water was a β-turn pattern for compounds **1**, **2**, **5**, and **7** (Table 2 and Figures S4 to S11), whose position 3 has D-Leu in common. For compound **2**, the locked β-turn pattern for the FEL of molecular shape was relatively tight with only side-chains freely rotating, compared to the other compounds. (The flexibility of the compounds will be discussed later.)

3.4 Relation between the 3D properties and cell permeability.

Cell permeability is plotted vs. the average SASA and PSA in Figure 7. The average SASA in cyclohexane showed excellent correlation with cell permeability (R^2 = 0.872), whereas the correlation was weaker in chloroform (R^2 = 0.39) and water (R^2 = 0.426). These results indicate that compounds with smaller SASAs in cyclohexane are more permeable, and that cyclohexane provides a better overall *in silico* mimic for electronic factors affecting permeability within the cell membrane. In chloroform, the average SASAs of compounds **5** and **7** were higher than the others and these were not on the line showing good correlation. This is because larger conformational changes between β-turn and cage-like patterns occurred for compound **5** and between β-turn and collapsed β-turn patterns for compound **7** (See Figure 4b for backbone RMSD differences between representative structures). It is also interesting that the compounds exhibiting high permeability, especially compounds **7** and **8,** exhibited large differences in SASA in cyclohexane and water. Such large differences were also observed as a result of the changes in the FEL of molecular shape in cyclohexane and water (See Figure 5). From the FELs and Table 2, a cage-like pattern observed for compounds **1** to **5** in cyclohexane tended to be less permeable, while the collapsed β-turn pattern found for compounds **6** to **8** in cyclohexane was more permeable.

An excellent correlation between MDCK $logP_{app}$ and $logD_{hc/w}$ (*i.e.*, $logD_{dec/w}$; partition coefficient with 1,9-decadiene and $logD_{cyc/w}$; partition coefficent with cyclohexane) was reported,[30] and we confirmed the relation between these partition coefficents and surface areas (Figures 8 and S13). As expected, the average SASA in cyclohexane correlated well with $logD_{dec/w}$ (R^2 = 0.765) and $logD_{cyc/w}$ (R^2 = 0.605), whereas lower correlations were found in chloroform and water.

The average PSA did not correlate with cell permeability and $logD_{dec/w}$ in these hexapeptide diastereomers (Figure 7a–c, 8a–c, and S13a–c). The PSA is known to correlate with

permeability for bRo5 compounds;[33,69,70] however, the compounds we investigated exhibited similar PSA values for each solvent. In cyclohexane, polar groups were protected by forming transannular IMHB, resulting in an average PSA of around 1.40 nm^2, whereas in water, polar groups were exposed to water molecules, resulting in an average PSA of around 1.72 nm^2. In chloroform, all compounds had larger average PSAs than in cyclohexane, especially compounds **5** and **7** again, because these compounds tended to form the β-turn pattern, with more exposed polar amide NHs, compared to in cyclohexane.

3.5 Relation between the SASA and aqueous solubility.

Although the aqueous solubility range was narrow, the average SASA in water correlates well with the aqueous solubility (R^2 = 0.755) (Figure 9). Compound **2** had good solubility, however, as described above, the conformation was locked to the β-turn pattern whereas three amide hydrogens are exposed to the water resulting in the average PSA being relatively high. Less soluble compounds **4** and **8** were locked around a disk-like shape in the FELs of molecular shape (Figure 5c). These compounds also had lower polarity (*i.e.*, non-polar surface area; differences between SASA and PSA in Figure 7c and 7f), in comparison with the other compounds that can more easily access multiple other conformations with higher exposed polarity. However, this effect is less dramatic than the permeability effect.

3.6 Relation between conformation and PAMPA.

The range of PAMPA permeabilities for this series was relatively narrow compared to their cell permeabilities; the correlation between cell permeability and PAMPA was moderate (R^2 = 0.671). The most cell permeable compounds **7** and **8** also exhibited the highest PAMPA permeabilities. It is interesting that compounds **4** and **8**, structurally identical except at position 4, had nearly the same range of PAMPA values and solubility; however, the cell permeability differed by one order of magnitude. Position 4 affects the hydrogen bonding between the amide NH of D-Leu5 and oxygen of Leu3, corresponding to the matrix [5,3] in Figure 4; that is, compound **4** formed no hydrogen bond. A possible interpretation for this observation is that compound **4** forms a mixture of the cage-like pattern (type **A** in Figure 4) and collapsed β-turn pattern (type **D** in Figure 4) in cyclohexane and chloroform (Table 2 and Figure S7). Although the thermodynamic balance of both conformers varies depending on the solvents from the FEL, the cage-like pattern is slightly preferred. This cage-like pattern has two non-hydrogen bonded amide NH groups, one of these (Tyr6) being completely exposed to solvent while the other is protected by side-chains. Conversely, compound **8** only forms a collapsed β-turn (**E**) in cyclohexane and chloroform, in which no amide NH groups are exposed to the solvents. The exposure of one additional hydrogen bond donor (HBD) was reported to yield a penalty from −1.6 to −1.9 units in $\log D_{dec/w}$ in test compounds,[30] and the difference between **4** and **8** was −1.65, reinforcing the observed change in the HBD count.

3.7 Flexibility and overlap of the conformation calculated from the FEL.

The $Flex_{FEL}$ values are listed in Figure 5d from the molecular shape and Figure 6e from the PC-1 and PC-2 planes. The overall tendency of the values for the solvents was almost the same for Figures 5d and 6e, except for compounds **2**, **6**, and **8**. These compounds had the

same range of values among the solvents based on the molecular shape; however, compound **2** had a smaller value (i.e., rigid) and compounds **6** and **8** had a larger value (more flexible) in water based on the PC plane. It is obvious that the $Flex_{FEL}$ values alone could not distinguish the detailed difference between the molecular shapes; thus, we now focus on the values obtained from the PC plane. From Figure 6e, it was observed that flexibility increased in the order of cyclohexane, chloroform, and water. Compounds **3**, **4**, **6**, and **8** (whose position 3 has L-Leu in common) had small $Flex_{FEL}$ values in cyclohexane and chloroform; however, these increased in water. Compounds **1**, **5**, and **7** had small values in cyclohexane but larger values in chloroform and water. The order was only reversed for compound **2**. The $Flex_{FEL}$ values could be rationalized by the outliers of the SASA and cell permeability plotted in Figure 7d, where compound **3** had a small value (rigid) and **5** had a large value (flexible) in cyclohexane. Figure 7e also showed that the outliers for **5** and **7** had larger $Flex_{FEL}$ values, resulting in worse correlation in chloroform. The outliers for the SASA and solubility (compound **2** in Figure 9) could be attributed to the especially small $Flex_{FEL}$ value in water, in which the conformation is locked to the type **C** pattern resulting in a large average SASA.

The $overlaps_{s1\rightarrow s2}(z)$ along the threshold (z) of the PMF from the PC plane were plotted in Figure S15. It is convenient to divide the threshold region by 1.0 kcal/mol. From Figure S15c and S15f, most compounds reached a plateau at $z \approx 2$ kcal/mol, indicating almost identical conformations in cyclohexane and chloroform within this threshold. It is worth noting the sigmoidal profiles for compounds **5** and **7** (Figure S15f), resulting from the different stable conformations in these solvents. It is also found that the most permeable compound **8** has the sigmoidal profiles for water to cyclohexane or chloroform (Figure S15d and e). This profile may provide the insight into the possible design of the permeable compound from the overlap between the FELs.

3.8 Membrane permeation models.

Passive membrane permeation for cyclic peptides has been ascribed in part to their chameleonic properties, *i.e.*, their ability to adopt different conformations in different environments.[31–33] A conventional model suggests that permeation occurs for the most stable conformation in the membrane when it occasionally forms in water.[7] A congruent conformation model indicates that permeation is assisted by congruent conformations, which significantly populate in both water and the membrane.[8] Another model proposed by Craik and co-workers suggests that the ratios of conformational polymorphism between structures were different in each state, such as aqueous, membrane head group, and membrane tail.[29]

Considering these conformational observations in the light of the passive membrane permeation models, we speculated that the conformations of the compounds in water changed compared to those in cyclohexane via two different routes depending on the structures of compounds based on the thermodynamic properties. A conventional conformational model was supported for compound **8**, where the collapsed β-turn pattern region (**E** in Figure 6d) overlapped well among the solvents. A possible interpretation of such a model is that the collapsed β-turn pattern could form in water and permeate the membrane while in this conformation (Figure 10a). Conversely, a more complicated

permeation model was supported for compound **7**, where the collapsed β-turn pattern region (**E** in Figure 6d) overlaps between in cyclohexane and chloroform, but not in water. A possible interpretation of the mechanism is that the β-turn pattern (**C** in Figure 6d) is initially formed in water, and then, possibly near the water-membrane boundary, equilibration between the β-turn and collapsed β-turn patterns occurs, and membrane permeation is achieved via the collapsed β-turn pattern, which is thermodynamically more stable in cyclohexane (Figure 10b). It was also noted that the collapsed β-turn pattern did not form in water for compound **7** (See Table 2 and Figure 6 for details). Therefore, a single stereocenter change between compounds **7** and **8** (*i.e.,* position 3) reveals different possible conformational structural profiles related to permeability. (Further work is required to explore conformational dynamics not sampled by thermodynamic minima, *e.g.*, Ref. 9.)

3.9 Possible strategy for designing permeable cyclic peptides.

From the above results, a possible strategy for designing permeable cyclic peptides using McMD simulations is described in the flow chart in Figure 10c. Firstly, because the simulation timing is shorter in explicit chloroform than in cyclohexane and water, we propose running an initial simulation in explicit chloroform for designed cyclic peptides. Secondly, compounds that have the highest number of IMHBs are selected, rejecting any compounds that have exposed HBDs. Thirdly, simulation is performed in explicit cyclohexane and water for the cyclic peptides, and the FELs are compared at T = 300 K for each solvent. Fourthly, overlaps among the FELs are compared. Finally, the most overlapped compound among the solvents is selected. If no overlap occurs between solvents, the sequence is redesigned and repeated from the first step.

4. CONCLUSION

We performed the conformational analysis of eight cyclic hexapeptide diastereomers in explicit cyclohexane, chloroform, and water by McMD simulation. FELs of molecular shape and principal component axes were obtained at T = 300 K. Ensembles of each compound and solvent at T = 300 K were also obtained, and 3D properties, such as SASA and PSA, were calculated. A new flexibility index $Flex_{FEL}$ was introduced. A possible strategy for designing permeable cyclic peptides is described.

A single stereoisomeric change affects the conformational patterns, resulting in permeability and solubility differences. The average SASA in cyclohexane correlated well with cell permeability, and the average SASA in water correlated with the aqueous solubility. It is surprising that only a simple arithmetic average of SASA from the ensemble at T = 300 K represents such physical properties so well. It is emphasized that no further clustering or selection of individual conformers was required for each compound, even with multiple conformations present in the ensemble. It was also found that cyclohexane is better than chloroform for hydrophobic environments based on the permeability.

Flexibility is summarized as follows from the permeation models and correlations between SASAs and experimental values: increased flexibility is good to allow conformational overlap to achieve one of the permeation models, however, it is a property over-sampled by chloroform yielding some of the lesser correlations there.

Since the MW is the same for all the compounds we examined, we did not treat the size effect explicitly. The molecular shape contains no size information, because it is calculated from normalized PMI ratios. The size effect may be required for further investigation, e.g., correction by a radius of gyration or a volume of the conformation.

Although we only calculated the cyclic hexapeptide with L- or D-amino acid, it is possible to simulate *cis/trans* isomerization of N-methylated amino acid by McMD simulations with current protocols. The McMD simulations have the advantage that the reaction coordinate is only the potential energy, which is independent of the system size.

Supplementary Material

Refer to Web version on PubMed Central for supplementary material.

ACKNOWLEDGMENTS

The synthesis of the compounds for this work was supported by NIH award GM131135.

ABBREVIATIONS:

MD	molecular dynamics
McMD	multicanonical molecular dynamics
FEL	free energy landscape
MDCK	Madin-Darby canine kidney
PAMPA	parallel artificial membrane permeability assay
SASA	solvent accessible surface area
PSA	polar surface area
PCA	principal component analysis
IMHB	intramolecular hydrogen bond.
logD	experimental partition coefficient at pH 7.4

REFERENCES

(1). Chen I-J; Foloppe N Tackling the Conformational Sampling of Larger Flexible Compounds and Macrocycles in Pharmacology and Drug Discovery. Bioorg. Med. Chem. 2013, 21, 7898–7920. 10.1016/j.bmc.2013.10.003. [PubMed: 24184215]

(2). McHugh SM; Rogers JR; Solomon SA; Yu H; Lin Y-S Computational Methods to Design Cyclic Peptides. Curr. Opin. Chem. Biol. 2016, 34, 95–102. 10.1016/j.cbpa.2016.08.004. [PubMed: 27592259]

(3). Hosseinzadeh P; Bhardwaj G; Mulligan VK; Shortridge MD; Craven TW; Pardo-Avila F; Rettie SA; Kim DE; Silva D-A; Ibrahim YM; Webb IK; Cort JR; Adkins JN; Varani G; Baker D Comprehensive Computational Design of Ordered Peptide Macrocycles. Science 2017, 358, 1461–1466. 10.1126/science.aap7577. [PubMed: 29242347]

(4). Sindhikara D; Spronk SA; Day T; Borrelli K; Cheney DL; Posy SL Improving Accuracy, Diversity, and Speed with Prime Macrocycle Conformational Sampling. J. Chem. Inf. Model. 2017, 57, 1881–1894. 10.1021/acs.jcim.7b00052. [PubMed: 28727915]

(5). Poongavanam V; Danelius E; Peintner S; Alcaraz L; Caron G; Cummings MD; Wlodek S; Erdelyi M; Hawkins PCD; Ermondi G; Kihlberg J Conformational Sampling of Macrocyclic Drugs in Different Environments: Can We Find the Relevant Conformations? ACS Omega 2018, 3, 11742–11757. 10.1021/acsomega.8b01379. [PubMed: 30320271]

(6). Rezai T; Yu B; Millhauser GL; Jacobson MP; Lokey RS Testing the Conformational Hypothesis of Passive Membrane Permeability Using Synthetic Cyclic Peptide Diastereomers. J. Am. Chem. Soc. 2006, 128, 2510–2511. 10.1021/ja0563455. [PubMed: 16492015]

(7). Rezai T; Bock JE; Zhou MV; Kalyanaraman C; Lokey RS; Jacobson MP Conformational Flexibility, Internal Hydrogen Bonding, and Passive Membrane Permeability: Successful in Silico Prediction of the Relative Permeabilities of Cyclic Peptides. J. Am. Chem. Soc. 2006, 128, 14073–14080. 10.1021/ja063076p. [PubMed: 17061890]

(8). Witek J; Keller BG; Blatter M; Meissner A; Wagner T; Riniker S Kinetic Models of Cyclosporin A in Polar and Apolar Environments Reveal Multiple Congruent Conformational States. J. Chem. Inf. Model. 2016, 56, 1547–1562. 10.1021/acs.jcim.6b00251. [PubMed: 27387150]

(9). Witek J; Mühlbauer M; Keller BG; Blatter M; Meissner A; Wagner T; Riniker S Interconversion Rates between Conformational States as Rationale for the Membrane Permeability of Cyclosporines. ChemPhysChem 2017, 18, 3309–3314. 10.1002/cphc.201700995. [PubMed: 28921848]

(10). Witek J; Wang S; Schroeder B; Lingwood R; Dounas A; Roth H-J; Fouché M; Blatter M; Lemke O; Keller B; Riniker S Rationalization of the Membrane Permeability Differences in a Series of Analogue Cyclic Decapeptides. J. Chem. Inf. Model. 2019, 59, 294–308. 10.1021/acs.jcim.8b00485. [PubMed: 30457855]

(11). McHugh SM; Rogers JR; Yu H; Lin Y-S Insights into How Cyclic Peptides Switch Conformations. J. Chem. Theory Comput. 2016, 12, 2480–2488. 10.1021/acs.jctc.6b00193. [PubMed: 27031286]

(12). McHugh SM; Yu H; Slough DP; Lin Y-S Mapping the Sequence–Structure Relationships of Simple Cyclic Hexapeptides. Phys. Chem. Chem. Phys. 2017, 19, 3315–3324. 10.1039/C6CP06192C. [PubMed: 28091629]

(13). Cummings AE; Miao J; Slough DP; McHugh SM; Kritzer JA; Lin Y-S β-Branched Amino Acids Stabilize Specific Conformations of Cyclic Hexapeptides. Biophys. J. 2019, 116, 433–444. 10.1016/j.bpj.2018.12.015. [PubMed: 30661666]

(14). Kamenik AS; Lessel U; Fuchs JE; Fox T; Liedl KR Peptidic Macrocycles - Conformational Sampling and Thermodynamic Characterization. J. Chem. Inf. Model. 2018, 58, 982–992. 10.1021/acs.jcim.8b00097. [PubMed: 29652495]

(15). Sugita Y; Okamoto Y Replica-Exchange Molecular Dynamics Method for Protein Folding. Chem. Phys. Lett. 1999, 314, 141–151. 10.1016/S0009-2614(99)01123-9.

(16). Laio A; Parrinello M Escaping Free-Energy Minima. Proc. Natl. Acad. Sci. 2002, 99, 12562–12566. 10.1073/pnas.202427399. [PubMed: 12271136]

(17). Hamelberg D; Mongan J; McCammon JA Accelerated Molecular Dynamics: A Promising and Efficient Simulation Method for Biomolecules. J. Chem. Phys. 2004, 120, 11919–11929. 10.1063/1.1755656. [PubMed: 15268227]

(18). Nguyen QNN; Schwochert J; Tantillo DJ; Lokey RS Using 1H and 13C NMR Chemical Shifts to Determine Cyclic Peptide Conformations: A Combined Molecular Dynamics and Quantum Mechanics Approach. Phys. Chem. Chem. Phys. 2018, 20, 14003–14012. 10.1039/C8CP01616J. [PubMed: 29744489]

(19). Coutsias EA; Lexa KW; Wester MJ; Pollock SN; Jacobson MP Exhaustive Conformational Sampling of Complex Fused Ring Macrocycles Using Inverse Kinematics. J. Chem. Theory Comput. 2016, 12, 4674–4687. 10.1021/acs.jctc.6b00250. [PubMed: 27447193]

(20). Jusot M; Stratmann D; Vaisset M; Chomilier J; Cortés J Exhaustive Exploration of the Conformational Landscape of Small Cyclic Peptides Using a Robotics Approach. J. Chem. Inf. Model. 2018, 58, 2355–2368. 10.1021/acs.jcim.8b00375. [PubMed: 30299093]

(21). Nakajima N; Nakamura H; Kidera A Multicanonical Ensemble Generated by Molecular Dynamics Simulation for Enhanced Conformational Sampling of Peptides. J. Phys. Chem. B 1997, 101, 817–824. 10.1021/jp962142e.

(22). Nakajima N; Higo J; Kidera A; Nakamura H Free Energy Landscapes of Peptides by Enhanced Conformational Sampling. J. Mol. Biol. 2000, 296, 197–216. 10.1006/jmbi.1999.3440. [PubMed: 10656827]

(23). Ono S; Nakajima N; Higo J; Nakamura H Peptide Free-Energy Profile Is Strongly Dependent on the Force Field: Comparison of C96 and AMBER95. J. Comput. Chem. 2000, 21, 748–762. 10.1002/(SICI)1096-987X(20000715)21:9<748::AID-JCC4>3.0.CO;2-2.

(24). Higo J; Galzitskaya OV; Ono S; Nakamura H Energy Landscape of a β-Hairpin Peptide in Explicit Water Studied by Multicanonical Molecular Dynamics. Chem. Phys. Lett. 2001, 337, 169–175. 10.1016/S0009-2614(01)00118-X.

(25). Higo J; Nishimura Y; Nakamura H A Free-Energy Landscape for Coupled Folding and Binding of an Intrinsically Disordered Protein in Explicit Solvent from Detailed All-Atom Computations. J. Am. Chem. Soc. 2011, 133, 10448–10458. 10.1021/ja110338e. [PubMed: 21627111]

(26). Higo J; Umezawa K Free-Energy Landscape of Intrinsically Disordered Proteins Investigated by All-Atom Multicanonical Molecular Dynamics In Protein Conformational Dynamics; Han K, Zhang X, Yang M, Eds.; Springer International Publishing: Cham, 2014; Vol. 805, pp 331–351.

(27). Nishigami H; Kamiya N; Nakamura H Revisiting Antibody Modeling Assessment for CDR-H3 Loop. Protein Eng. Des. Sel. 2016, 29, 477–484. 10.1093/protein/gzw028. [PubMed: 27515703]

(28). Bekker G-J; Kamiya N; Araki M; Fukuda I; Okuno Y; Nakamura H Accurate Prediction of Complex Structure and Affinity for a Flexible Protein Receptor and Its Inhibitor. J. Chem. Theory Comput. 2017, 13, 2389–2399. 10.1021/acs.jctc.6b01127. [PubMed: 28482660]

(29). Wang CK; Swedberg JE; Harvey PJ; Kaas Q; Craik DJ Conformational Flexibility Is a Determinant of Permeability for Cyclosporin. J. Phys. Chem. B 2018, 122, 2261–2276. 10.1021/acs.jpcb.7b12419. [PubMed: 29400464]

(30). Naylor MR; Ly AM; Handford MJ; Ramos DP; Pye CR; Furukawa A; Klein VG; Noland RP; Edmondson Q; Turmon AC; Hewitt WM; Schwochert J; Townsend CE; Kelly CN; Blanco M-J; Lokey RS Lipophilic Permeability Efficiency Reconciles the Opposing Roles of Lipophilicity in Membrane Permeability and Aqueous Solubility. J. Med. Chem. 2018, 61, 11169–11182. 10.1021/acs.jmedchem.8b01259. [PubMed: 30395703]

(31). Whitty A; Zhong M; Viarengo L; Beglov D; Hall DR; Vajda S Quantifying the Chameleonic Properties of Macrocycles and Other High-Molecular-Weight Drugs. Drug Discov. Today 2016, 21, 712–717. 10.1016/j.drudis.2016.02.005. [PubMed: 26891978]

(32). Schwochert J; Lao Y; Pye CR; Naylor MR; Desai PV; Gonzalez Valcarcel IC; Barrett JA; Sawada G; Blanco M-J; Lokey RS Stereochemistry Balances Cell Permeability and Solubility in the Naturally Derived Phepropeptin Cyclic Peptides. ACS Med. Chem. Lett 2016, 7, 757–761. 10.1021/acsmedchemlett.6b00100. [PubMed: 27563399]

(33). Rossi Sebastiano M; Doak BC; Backlund M; Poongavanam V; Over B; Ermondi G; Caron G; Matsson P; Kihlberg J Impact of Dynamically Exposed Polarity on Permeability and Solubility of Chameleonic Drugs Beyond the Rule of 5. J. Med. Chem. 2018, 61, 4189–4202. 10.1021/acs.jmedchem.8b00347. [PubMed: 29608068]

(34). Hewitt WM; Leung SSF; Pye CR; Ponkey AR; Bednarek M; Jacobson MP; Lokey RS Cell-Permeable Cyclic Peptides from Synthetic Libraries Inspired by Natural Products. J. Am. Chem. Soc. 2015, 137, 715–721. 10.1021/ja508766b. [PubMed: 25517352]

(35). Ertl P; Rohde B; Selzer P Fast Calculation of Molecular Polar Surface Area as a Sum of Fragment-Based Contributions and Its Application to the Prediction of Drug Transport Properties. J. Med. Chem. 2000, 43, 3714–3717. 10.1021/jm000942e. [PubMed: 11020286]

(36). Ghose AK; Crippen GM Atomic Physicochemical Parameters for Three-Dimensional Structure-Directed Quantitative Structure-Activity Relationships I. Partition Coefficients as a Measure of Hydrophobicity. J. Comput. Chem. 1986, 7, 565–577. 10.1002/jcc.540070419.

(37). Di L; Whitney-Pickett C; Umland JP; Zhang H; Zhang X; Gebhard DF; Lai Y; Federico JJ; Davidson RE; Smith R; Reyner EL; Lee C; Feng B; Rotter C; Varma MV; Kempshall S; Fenner K; El-kattan AF; Liston TE; Troutman MD Development of a New Permeability Assay Using

Low-efflux MDCKII Cells. J. Pharm. Sci. 2011, 100, 4974–4985. 10.1002/jps.22674. [PubMed: 21766308]

(38). Marelli UK; Ovadia O; Frank AO; Chatterjee J; Gilon C; Hoffman A; Kessler H Cis-Peptide Bonds: A Key for Intestinal Permeability of Peptides? Chem. – Eur. J 2015, 21, 15148–15152. 10.1002/chem.201501600. [PubMed: 26337831]

(39). Wang CK; Northfield SE; Colless B; Chaousis S; Hamernig I; Lohman R-J; Nielsen DS; Schroeder CI; Liras S; Price DA; Fairlie DP; Craik DJ Rational Design and Synthesis of an Orally Bioavailable Peptide Guided by NMR Amide Temperature Coefficients. Proc. Natl. Acad. Sci. 2014, 111, 17504–17509. 10.1073/pnas.1417611111. [PubMed: 25416591]

(40). Räder AFB; Reichart F; Weinmüller M; Kessler H Improving Oral Bioavailability of Cyclic Peptides by N-Methylation. Bioorg. Med. Chem. 2018, 26, 2766–2773. 10.1016/j.bmc.2017.08.031. [PubMed: 28886995]

(41). Yu H; Lin Y-S Toward Structure Prediction of Cyclic Peptides. Phys. Chem. Chem. Phys. 2015, 17, 4210–4219. 10.1039/C4CP04580G. [PubMed: 25566700]

(42). Geng H; Jiang F; Wu Y-D Accurate Structure Prediction and Conformational Analysis of Cyclic Peptides with Residue-Specific Force Fields. J. Phys. Chem. Lett 2016, 1805–1810. 10.1021/acs.jpclett.6b00452. [PubMed: 27128113]

(43). Duan Y; Wu C; Chowdhury S; Lee MC; Xiong G; Zhang W; Yang R; Cieplak P; Luo R; Lee T; Caldwell J; Wang J; Kollman P A Point-Charge Force Field for Molecular Mechanics Simulations of Proteins Based on Condensed-Phase Quantum Mechanical Calculations. J. Comput. Chem. 2003, 24, 1999–2012. 10.1002/jcc.10349. [PubMed: 14531054]

(44). Molecular Operating Environment (MOE); Chemical Computing Group ULC, 1010 Sherbooke St. West, Suite #910, Montreal, QC, Canada, H3A 2R7, 2018.

(45). Labute P LowModeMD—Implicit Low-Mode Velocity Filtering Applied to Conformational Search of Macrocycles and Protein Loops. J. Chem. Inf. Model. 2010, 50, 792–800. 10.1021/ci900508k. [PubMed: 20429574]

(46). Martínez L; Andrade R; Birgin EG; Martínez JM PACKMOL: A Package for Building Initial Configurations for Molecular Dynamics Simulations. J. Comput. Chem. 2009, 30, 2157–2164. 10.1002/jcc.21224. [PubMed: 19229944]

(47). Jorgensen WL; Chandrasekhar J; Madura JD; Impey RW; Klein ML Comparison of Simple Potential Functions for Simulating Liquid Water. J. Chem. Phys. 1983, 79, 926–935. 10.1063/1.445869.

(48). Case DA; Cerutti DS; Cheatham TE III; Darden TA; Duke RE; Giese TJ; Gohlke H; Goetz AW; Greene D; Homeyer N; Izadi S; Kovalenko A; Lee TS; LeGrand S; Li P; Lin C; Liu J; Luchko T; Luo R; Mermelstein D; Merz KM; Monard G; Nguyen H; Omelyan I; Onufriev A; Pan F; Qi R; Roe DR; Roitberg A; Sagui C; Simmerling CL; Botello-Smith WM; Swails J; Walker RC; Wang J; Wolf RM; Wu X; Xiao L; York DM; Kollman PA AMBER 2017; University of California, San Francisco, 2017.

(49). Dickson CJ; Madej BD; Skjevik ÅA; Betz RM; Teigen K; Gould IR; Walker RC Lipid14: The Amber Lipid Force Field. J. Chem. Theory Comput. 2014, 10, 865–879. 10.1021/ct4010307. [PubMed: 24803855]

(50). Dupradeau F-Y; Pigache A; Zaffran T; Savineau C; Lelong R; Grivel N; Lelong D; Rosanski W; Cieplak P The R.E.D. Tools: Advances in RESP and ESP Charge Derivation and Force Field Library Building. Phys. Chem. Chem. Phys. 2010, 12, 7821–7839. 10.1039/C0CP00111B. [PubMed: 20574571]

(51). Berendsen HJC; Postma JPM; van Gunsteren WF; DiNola A; Haak JR Molecular Dynamics with Coupling to an External Bath. J. Chem. Phys. 1984, 81, 3684 10.1063/1.448118.

(52). Higo J; Kamiya N; Sugihara T; Yonezawa Y; Nakamura H Verifying Trivial Parallelization of Multicanonical Molecular Dynamics for Conformational Sampling of a Polypeptide in Explicit Water. Chem. Phys. Lett. 2009, 473, 326–329. 10.1016/j.cplett.2009.03.077.

(53). Higo J; Umezawa K; Nakamura H A Virtual-System Coupled Multicanonical Molecular Dynamics Simulation: Principles and Applications to Free-Energy Landscape of Protein–Protein Interaction with an All-Atom Model in Explicit Solvent. J. Chem. Phys. 2013, 138, 184106 10.1063/1.4803468. [PubMed: 23676028]

(54). Bussi G; Donadio D; Parrinello M Canonical Sampling through Velocity Rescaling. J. Chem. Phys. 2007, 126, 014101 10.1063/1.2408420. [PubMed: 17212484]

(55). Hess B; Bekker H; Berendsen HJC; Fraaije JGEM LINCS: A Linear Constraint Solver for Molecular Simulations. J. Comput. Chem. 1997, 18, 1463–1472. 10.1002/(SICI)1096-987X(199709)18:12<1463::AID-JCC4>3.0.CO;2-H.

(56). Roux B The Calculation of the Potential of Mean Force Using Computer Simulations. Comput. Phys. Commun. 1995, 91, 275–282. 10.1016/0010-4655(95)00053-I.

(57). Van Der Spoel D; Lindahl E; Hess B; Groenhof G; Mark AE; Berendsen HJC GROMACS: Fast, Flexible, and Free. J. Comput. Chem. 2005, 26, 1701–1718. 10.1002/jcc.20291. [PubMed: 16211538]

(58). Tubiana T; Carvaillo J-C; Boulard Y; Bressanelli S TTClust: A Versatile Molecular Simulation Trajectory Clustering Program with Graphical Summaries. J. Chem. Inf. Model. 2018, 58, 2178–2182. 10.1021/acs.jcim.8b00512. [PubMed: 30351057]

(59). Ward JH Jr Hierarchical Grouping to Optimize an Objective Function. J. Am. Stat. Assoc. 1963, 58, 236–244. 10.1080/01621459.1963.10500845.

(60). Humphrey W; Dalke A; Schulten K VMD: Visual Molecular Dynamics. J. Mol. Graph. 1996, 14, 33–38. [PubMed: 8744570]

(61). Sauer WHB; Schwarz MK Molecular Shape Diversity of Combinatorial Libraries: A Prerequisite for Broad Bioactivity. J. Chem. Inf. Comput. Sci. 2003, 43, 987–1003. 10.1021/ci025599w. [PubMed: 12767158]

(62). Ono S; Nakajima N; Higo J; Nakamura H The Multicanonical Weighted Histogram Analysis Method for the Free-Energy Landscape along Structural Transition Paths. Chem. Phys. Lett. 1999, 312, 247–254. 10.1016/S0009-2614(99)00969-0.

(63). Neale C; Pomès R; García AE Peptide Bond Isomerization in High-Temperature Simulations. J. Chem. Theory Comput. 2016, 12, 1989–1999. 10.1021/acs.jctc.5b01022. [PubMed: 26866899]

(64). Cierpicki T; Otlewski J Amide Proton Temperature Coefficients as Hydrogen Bond Indicators in Proteins. J. Biomol. NMR 2001, 21, 249–261. 10.1023/A:1012911329730. [PubMed: 11775741]

(65). Ghadiri MR; Granja JR; Milligan RA; McRee DE; Khazanovich N Self-Assembling Organic Nanotubes Based on a Cyclic Peptide Architecture. Nature 1993, 366, 324–327. 10.1038/366324a0. [PubMed: 8247126]

(66). Brea RJ; Reiriz C; Granja JR Towards Functional Bionanomaterials Based on Self-Assembling Cyclic Peptide Nanotubes. Chem. Soc. Rev. 2010, 39, 1448–1456. 10.1039/B805753M. [PubMed: 20419200]

(67). Rodríguez-Vázquez N; Amorín M; Granja JR Recent Advances in Controlling the Internal and External Properties of Self-Assembling Cyclic Peptide Nanotubes and Dimers. Org. Biomol. Chem. 2017, 15, 4490–4505. 10.1039/C7OB00351J. [PubMed: 28375421]

(68). Hayward S Peptide-Plane Flipping in Proteins. Protein Sci. 2001, 10, 2219–2227. 10.1110/ps.23101. [PubMed: 11604529]

(69). Guimarães CRW; Mathiowetz AM; Shalaeva M; Goetz G; Liras S Use of 3D Properties to Characterize Beyond Rule-of-5 Property Space for Passive Permeation. J. Chem. Inf. Model. 2012, 52, 882–890. 10.1021/ci300010y. [PubMed: 22394163]

(70). Giordanetto F; Kihlberg J Macrocyclic Drugs and Clinical Candidates: What Can Medicinal Chemists Learn from Their Properties? J. Med. Chem. 2014, 57, 278–295. 10.1021/jm400887j. [PubMed: 24044773]

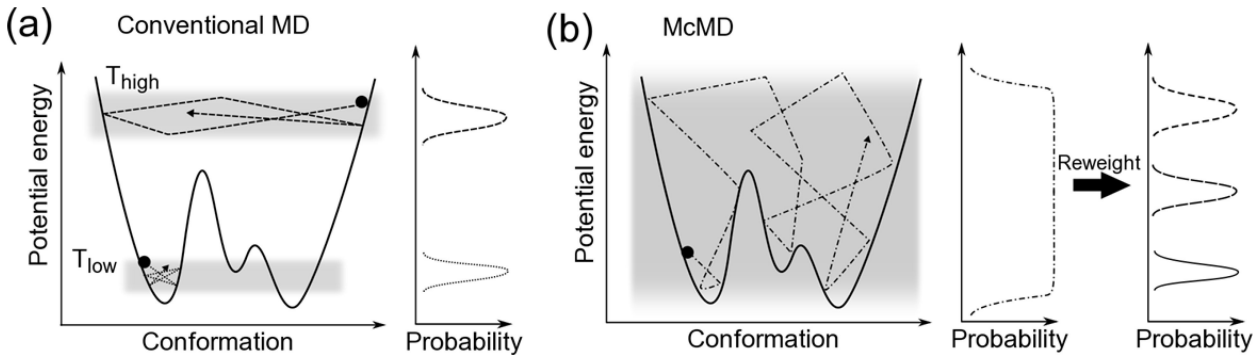

Figure 1.

Schematic view of conformational space and potential energy. Filled circles indicate initial structures. (a) Conventional MD performed at low temperature would be trapped at a local minimum and could not overcome the large potential energy barrier. High temperature MD samples a wider conformational space and overcomes large barriers; however, the structures are unrealistic. (b) McMD can equally sample a full potential energy space, easily overcome large barriers, and sample any local minima. Therefore, the staring conformation does not affect the results. After a production McMD run, canonical ensembles between low and high temperature states are easily obtained by reweighting.

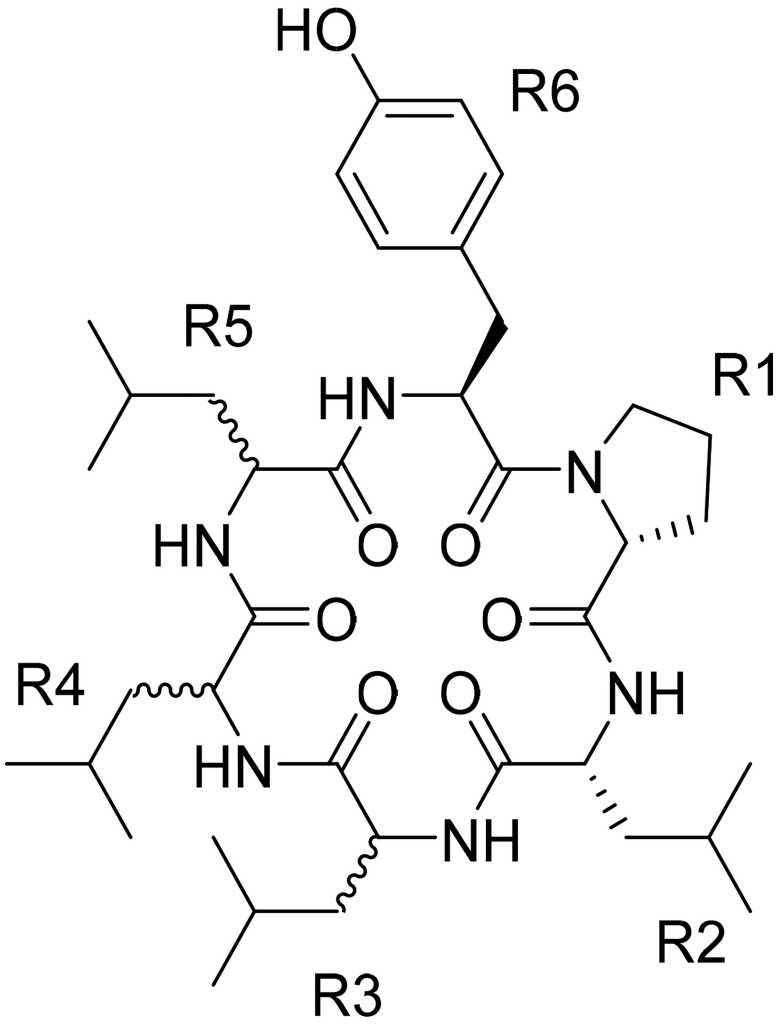

Figure 2.
Cyclic hexapeptide diastereomers.

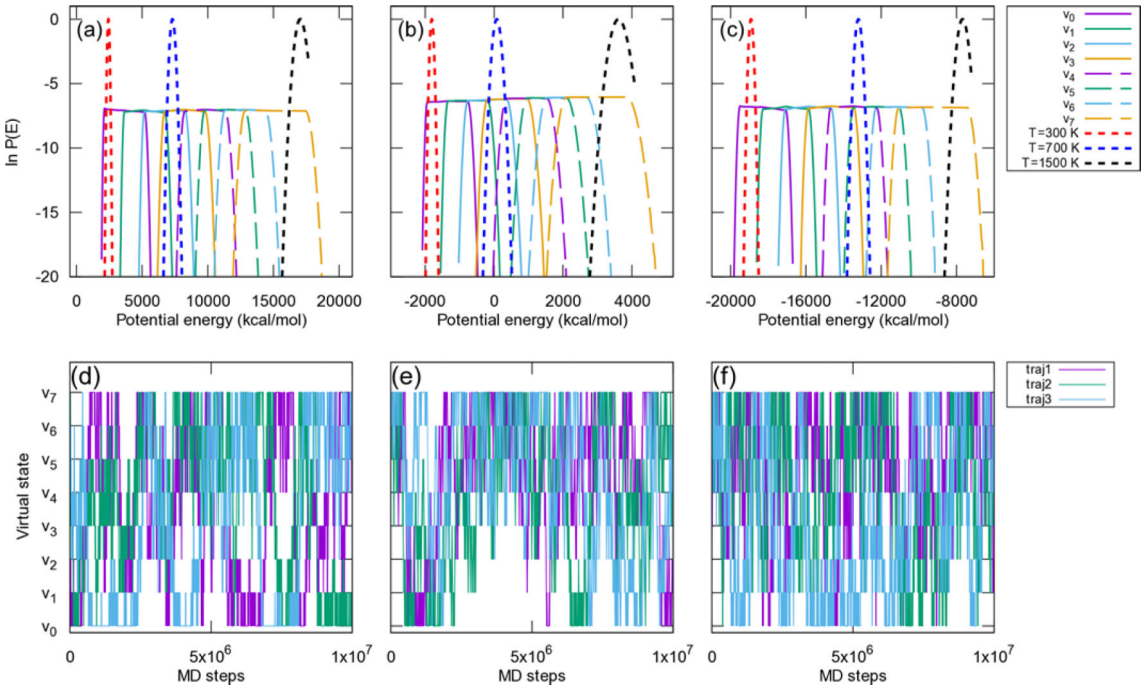

Figure 3.

Flat potential energy distribution of compound **8** for virtual states (v_0 to v_7) and reweighted canonical ensembles at T = 300, 700, and 1500 K. (a) in cyclohexane, (b) in chloroform and (c) in water. The exchange among virtual states for trajectories 1 to 3 out of 336 trajectories are shown for (d) in cyclohexane, (e) in chloroform and (f) in water. The following virtual state ranges were used: v_0 = [0.0, 0.2], v_1 = [0.1, 0.3], v_2 = [0.2, 0.4], v_3 = [0.3, 0.5], v_4 = [0.4, 0.6], v_5 = [0.5, 0.7], v_6 = [0.6, 0.8], and v_7 = [0.7, 1.0].

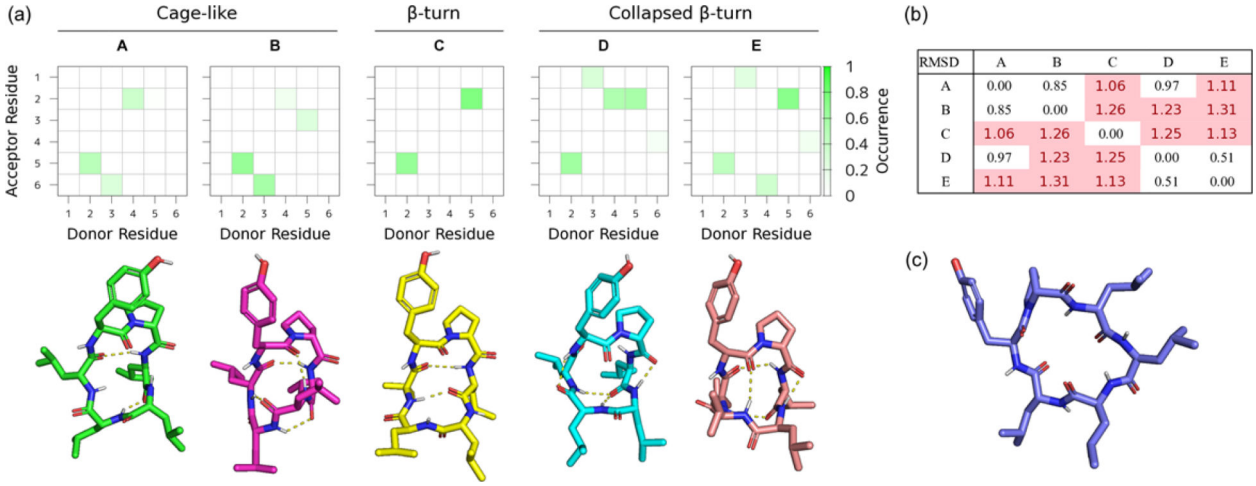

RMSD	A	B	C	D	E
A	0.00	0.85	1.06	0.97	1.11
B	0.85	0.00	1.26	1.23	1.31
C	1.06	1.26	0.00	1.25	1.13
D	0.97	1.23	1.25	0.00	0.51
E	1.11	1.31	1.13	0.51	0.00

Figure 4.

(a) Backbone hydrogen bond patterns and representative structures. Cage-like pattern (type **A** and **B**), β-turn pattern (type **C**), and collapsed β-turn pattern (types **D** and **E**). Structures $\mathbf{2}_{C1}$, $\mathbf{3}_{C1}$, $\mathbf{7}_{C1}$, $\mathbf{2}_{X1}$, and $\mathbf{8}_{C1}$ correspond to types **A**, **B**, **C**, **D**, and **E**, respectively. The subscript indicates the solvent and cluster names, where C1 is the first cluster in chloroform and X1 is the first cluster in cyclohexane. The color fade is defined by the occurrence of H-bonds obtained by the VMD H-bond plug-in for each cluster. (b) Backbone RMSD matrix between the representative structures. Highlights by red shades are larger than 1.00 Å. (c) Example of nIMHB = 0 and disk-like conformation **8** found in water.

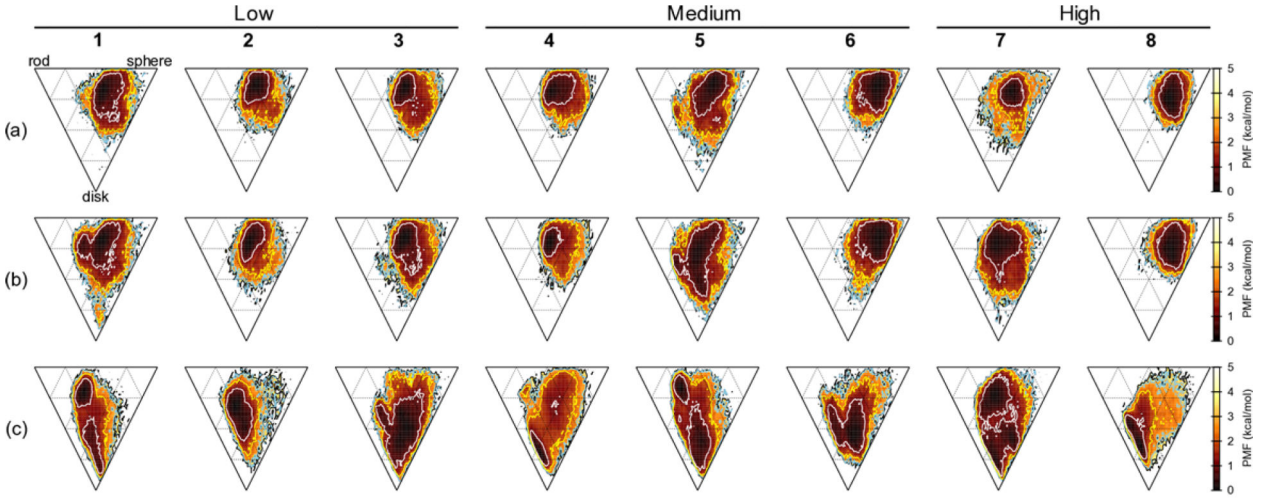

(d)

$Flex_{FEL}$	1	2	3	4	5	6	7	8
cyclohexane	1.535	0.879	1.051	1.321	1.965	1.413	0.740	0.906
chloroform	2.177	0.855	1.588	0.744	2.902	2.043	2.299	1.162
water	2.004	1.327	3.411	2.035	4.138	2.230	4.888	1.075

Figure 5.

FEL of molecular shape at T = 300 K for each compound and solvent. Each vertex, top left, top right and bottom represents a rod, sphere and disk, respectively. Annotated above for the permeability class defined in Table 1. (a) is in cyclohexane, (b) in chloroform, and (c) in water. The contour lines for PMF = 1.0, 2.0, 3.0, and 4.0 kcal/mol are plotted as white, yellow, sky-blue, and black lines, respectively. (d) $Flex_{FEL}$ values for each compound and solvent defined by the molecular shape plane.

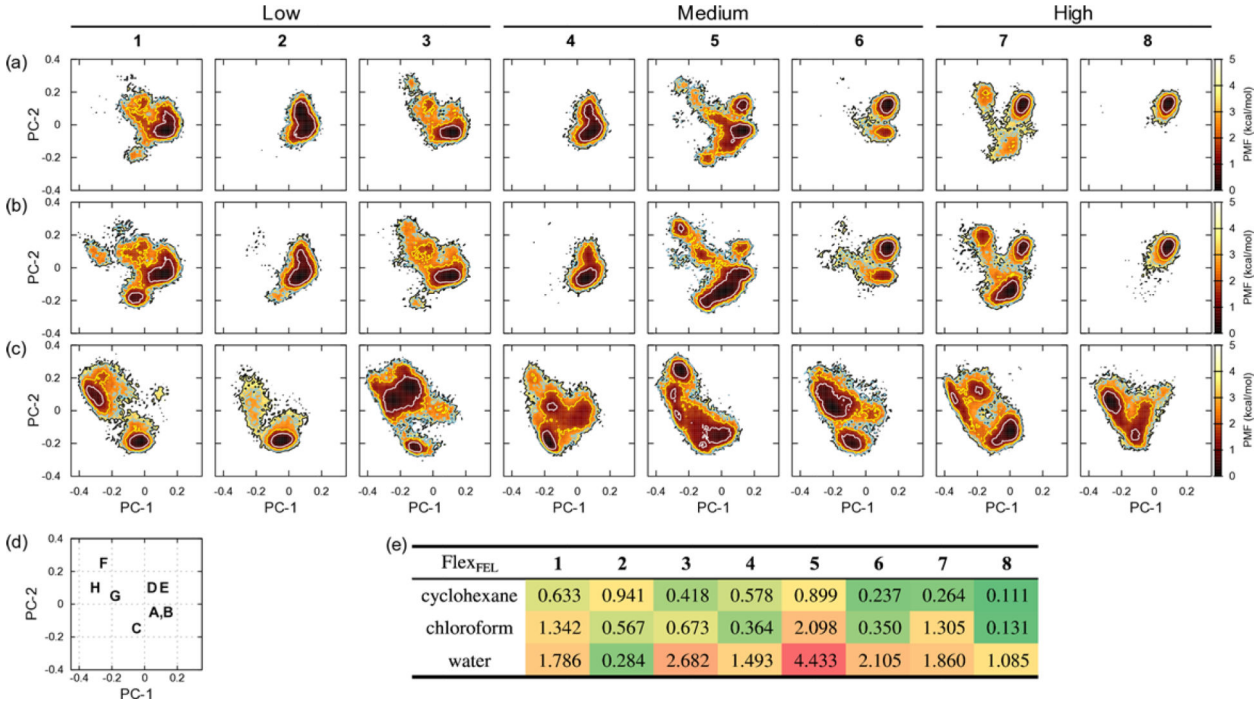

$Flex_{FEL}$	1	2	3	4	5	6	7	8
cyclohexane	0.633	0.941	0.418	0.578	0.899	0.237	0.264	0.111
chloroform	1.342	0.567	0.673	0.364	2.098	0.350	1.305	0.131
water	1.786	0.284	2.682	1.493	4.433	2.105	1.860	1.085

Figure 6.

FEL by PCA axis PC-1 vs. PC-2 at T = 300 K for each compound and solvent. Annotated above for the permeability class defined in Table 1. (a) is in cyclohexane, (b) in chloroform, and (c) in water. The contour lines for PMF = 1.0, 2.0, 3.0, and 4.0 kcal/mol are plotted as white, yellow, sky-blue, and black lines, respectively. (d) A representative box showing the locations of each pattern. See main text for details. (e) $Flex_{FEL}$ values for each compound and solvent defined by PC-1 and PC-2 planes.

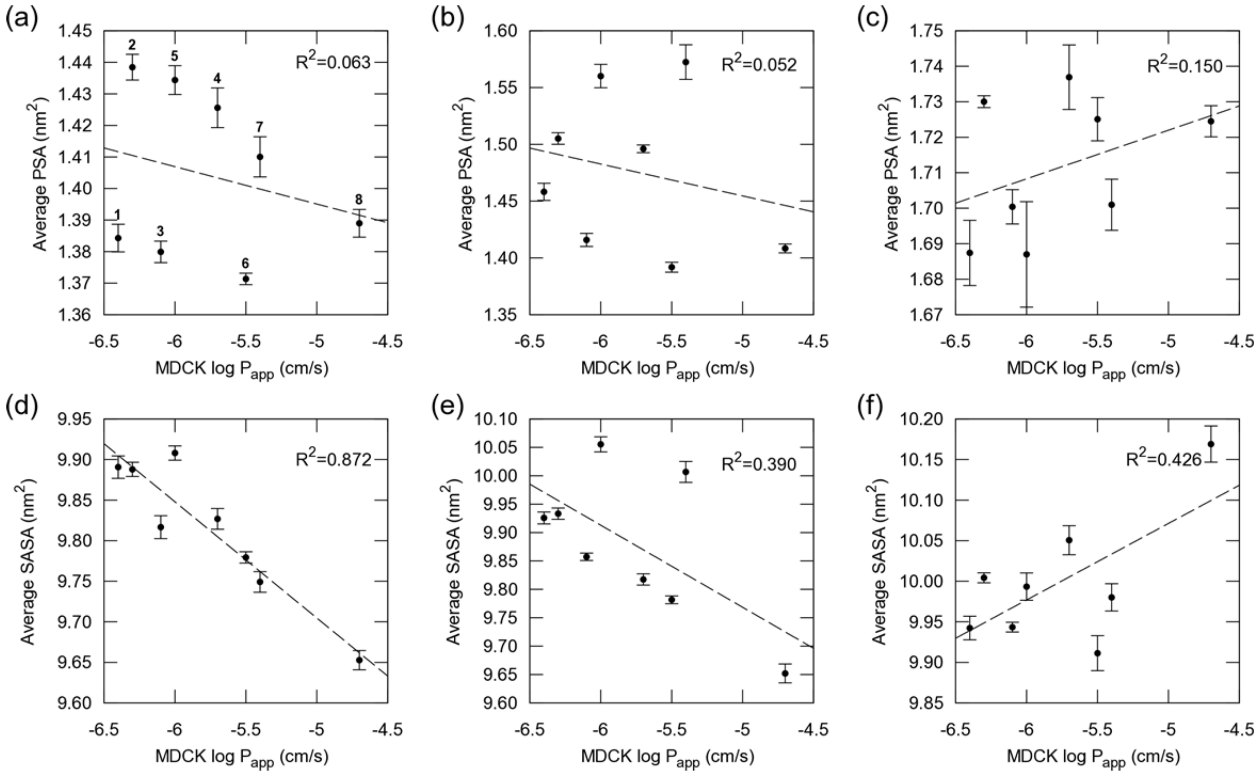

Figure 7.

Cell permeability vs. average PSA and SASA. (a) and (d) are in cyclohexane, (b) and (e) in chloroform, and (c) and (f) in water. Dashed lines are fitted for each point.

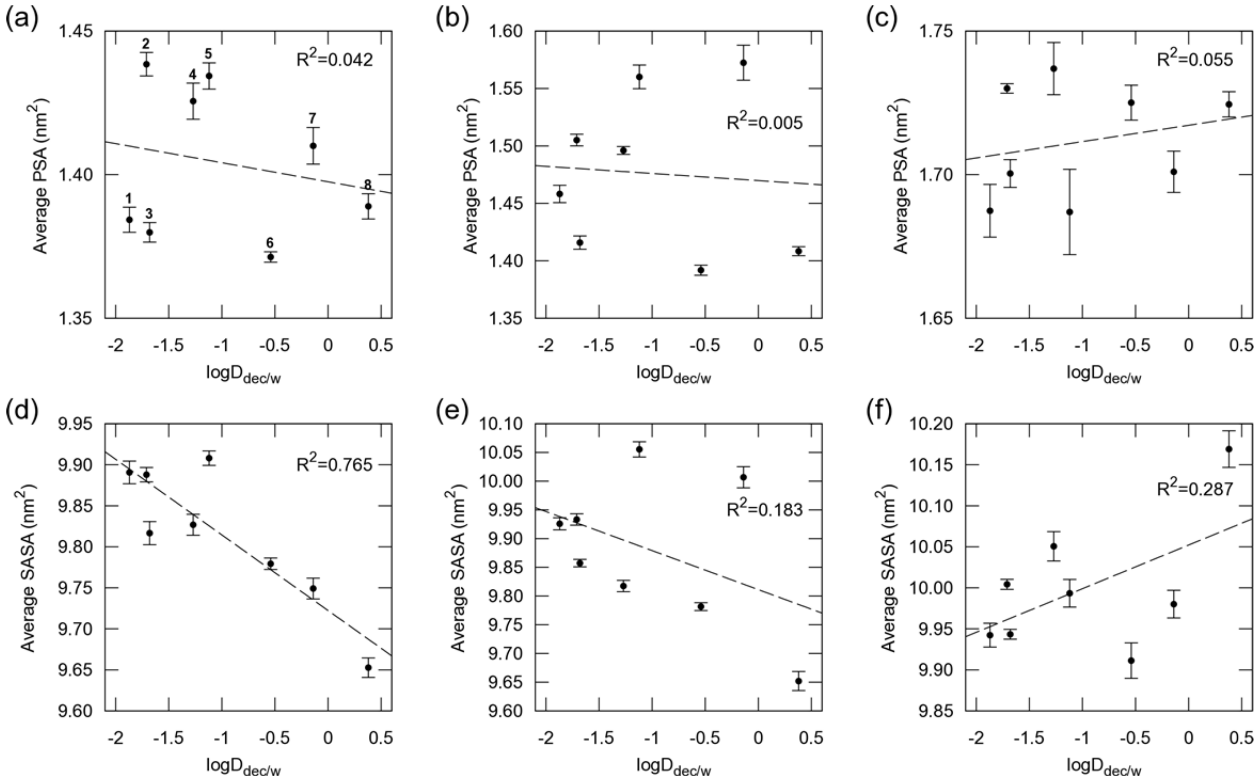

Figure 8.

$LogD_{dec/w}$ vs. average SASA and PSA. (a) and (d) are in cyclohexane, (b) and (e) in chloroform, and (c) and (f) in water. Dashed lines are fitted for each point.

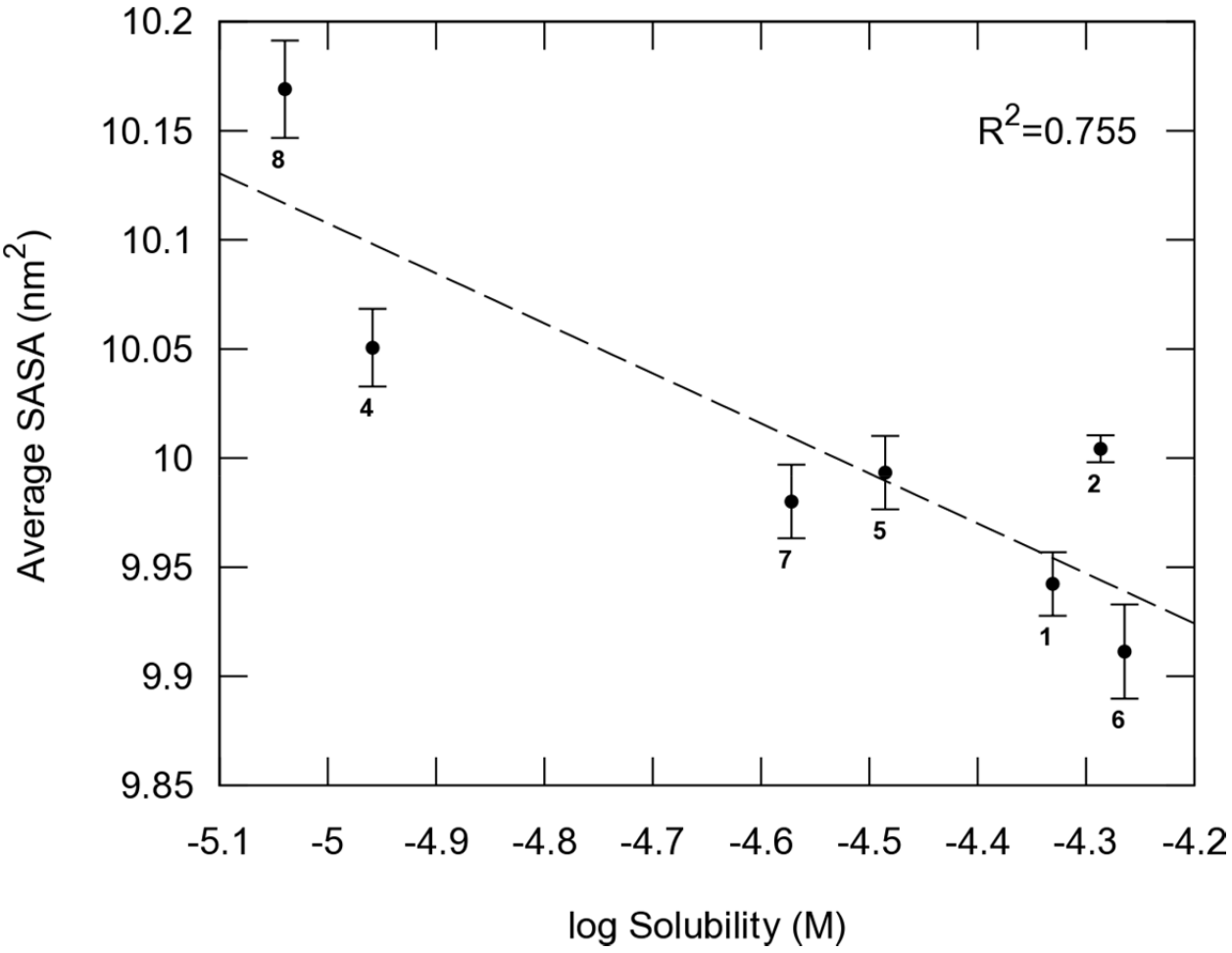

Figure 9.
Aqueous solubility vs. average SASA in water. Dashed lines are fitted for each point.

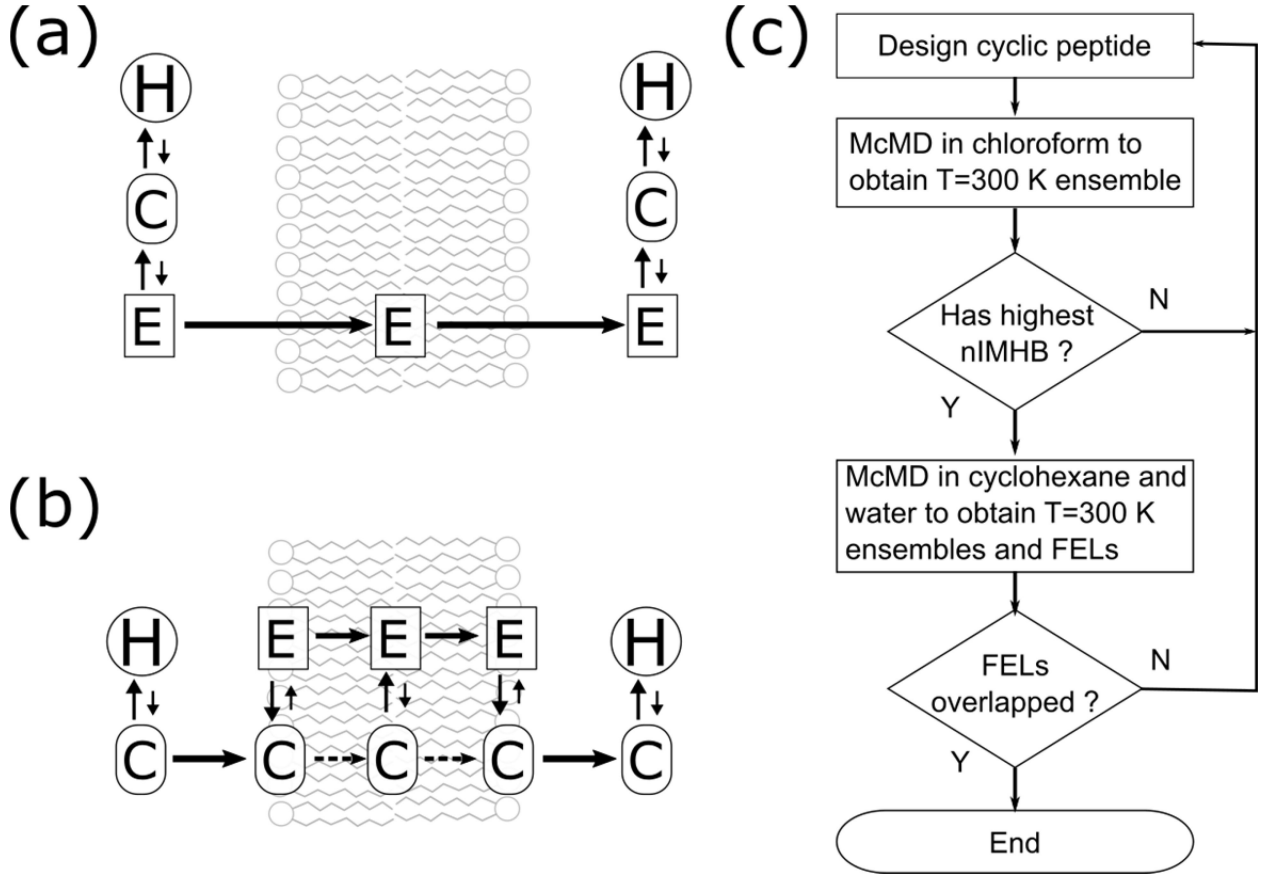

Figure 10.

Possible membrane permeation mechanisms. (a) Mechanism for compound **8**. Character **C**, **E**, and **H** denote conformation patterns in Figure 6d. (b) Mechanism for compound **7**. Note that pattern **E** could not form in water. (c) Flow chart of proposed strategy for designing permeable cyclic peptides.

Table 1.

Sequence, permeability and aqueous solubility data for each compound.

ID	R1	R2	R3	R4	R5	R6	MDCK		PAMPA	Sol.[a,c]
							P_{app}[a,b]	Class	P_{app}[b]	
1	D-Pro	D-Leu	D-Leu	D-Leu	L-Leu	L-Tyr	0.4	low	2.27	47
2	D-Pro	D-Leu	D-Leu	D-Leu	D-Leu	L-Tyr	0.5	low	2.87	52
3	D-Pro	D-Leu	L-Leu	D-Leu	L-Leu	L-Tyr	0.8	low	1.71	--[d]
4	D-Pro	D-Leu	L-Leu	D-Leu	D-Leu	L-Tyr	1.9	medium	4.92	11
5	D-Pro	D-Leu	D-Leu	L-Leu	L-Leu	L-Tyr	1	medium	1.66	33
6	D-Pro	D-Leu	L-Leu	L-Leu	L-Leu	L-Tyr	2.8	medium	2.59	54
7	D-Pro	D-Leu	D-Leu	L-Leu	D-Leu	L-Tyr	4	high	7.18	27
8	D-Pro	D-Leu	L-Leu	L-Leu	D-Leu	L-Tyr	19.3	high	7.74	9.1

[a] From Ref. 30.

[b] In units of 10^{-6} (cm/s).

[c] Aqueous Solubility pH 7.4 (μM).

[d] not determined.

Table 2.

Population of the patterns for each compound and solvent.

ID	Solvent	Population of the pattern (%)					
		Cage-like		β-turn	Collapsed β-turn		Minor clusters[b]
		A	B	C	D	E	
1	Cyclohexane	--[a]	57.4 ± 4.1	0.8 ± 1.1	28.2 ± 3.2	--[a]	13.6
	chloroform	--[a]	55.4 ± 2.0	18.9 ± 2.7	14.2 ± 1.4	--[a]	11.5
	water	--[a]	--[a]	49.4 ± 3.7	--[a]	--[a]	50.6
2	Cyclohexane	22.5 ± 8.3	--[a]	--[a]	65.4 ± 9.8	--[a]	12.1
	chloroform	56.3 ± 5.4	--[a]	0.6 ± 0.7	26.7 ± 3.3	--[a]	16.4
	water	--[a]	--[a]	45.5 ± 7.1	--[a]	--[a]	54.5
3	Cyclohexane	--[a]	76.5 ± 4.1	--[a]	5.9 ± 2.9	--[a]	17.5
	chloroform	--[a]	72.8 ± 6.9	--[a]	5.3 ± 3.2	--[a]	21.9
	water	--[a]	--[a]	10.8 ± 1.4	--[a]	--[a]	89.2
4	Cyclohexane	49.6 ± 2.6	--[a]	--[a]	21.6 ± 5.2	--[a]	28.7
	chloroform	79.3 ± 4.2	--[a]	--[a]	10.5 ± 3.6	--[a]	10.2
	water	23.2 ± 3.7	--[a]	45.0 ± 3.9	--[a]	--[a]	31.8
5	Cyclohexane	--[a]	48.1 ± 4.9	2.7 ± 3.3	--[a]	18.2 ± 6.2	31.0
	chloroform	--[a]	24.1 ± 3.5	38.7 ± 5.6	--[a]	--[a]	37.2
	water	--[a]	--[a]	44.5 ± 3.7	--[a]	--[a]	55.5
6	Cyclohexane	--[a]	13.1 ± 2.1	--[a]	--[a]	86.3 ± 1.8	0.5
	chloroform	--[a]	16.8 ± 3.8	--[a]	--[a]	79.0 ± 3.0	4.2
	water	--[a]	--[a]	--[a]	--[a]	--[a]	100.0
7	Cyclohexane	--[a]	--[a]	6.5 ± 2.1	--[a]	80.4 ± 3.8	13.1
	chloroform	--[a]	--[a]	57.2 ± 4.0	--[a]	24.8 ± 6.4	18.0
	water	--[a]	--[a]	37.8 ± 1.7	--[a]	--[a]	62.2
8	Cyclohexane	--[a]	--[a]	--[a]	--[a]	99.0 ± 0.5	1.0
	chloroform	--[a]	--[a]	--[a]	--[a]	90.8 ± 2.9	9.2
	water	--[a]	--[a]	25.9 ± 4.5	--[a]	5.6 ± 1.1	68.5

[a] not classified by the pattern.

[b] Includes major clusters found in water.